A Study of Cutting Temperatures in Turning Glass-Fiber-Reinforced -Plastic (GFRP) Composites with nose radius worn tools

Chung-Shin Chang*

*Dept. of Mechanical Engineering, National Ilan University, I-Lan, Taiwan, 260

cschang@niu.edu.tw

ABSTRACT

Nine kinds of chamfered main cutting edge carbide tools were used in turning of glass-fiber-reinforced plastics (GFRP) materials to study the temperature of tip's surface and the cutting forces. The friction forces and frictional heat generated on elementary cutting tools are calculated by using the measured cutting forces and the oblique cutting analysis. The heat partition factors between the tip and chip are solved by using the inverse heat transfer analysis, which utilizes temperature on the carbide tip's surface measured by infrared as the input. The tip's surface temperature of the carbide is solved by finite element analysis (FEA) and compared with those obtained from experimental measurements. A good agreement demonstrates the accuracy of the proposed model.

Keywords: FEA, GFRP, Nose radius and Temperature of GFRP

1 INTRODUCTION

Polymeric materials such as fiber reinforced plastics (FRP) have been widely used in various engineering structures. GFRP has been successfully used in the aerospace, transportation, recreational, appliance, electrical equipment, tank and piping industries [1]. The machining of glass fiber-epoxy composite materials is not the same as the machining of conventional metal materials. Singamneni [2] demonstrated the mixed finite and boundary element method (FEM) finally enables the estimation of the cutting temperatures which is a simple, efficient method, and at the same time it is quite easy to be implemented. The objective of this paper is to set up an oblique cutting GFRP model to study the cutting temperature for a nose radius worn tool with a chamfered main cutting edge.

2 THEORETICAL ANALYSES

For the case of chamfered main cutting edge, must have not only nose radius R, worn depths d_B, cutting depth d, feed rate f, cutting speed V, back rake angle α_b, side cutting edge angle C_s, end side cutting edge angle C_e, negative side rake angle, α_{S1} and positive rake angle α_{S2} are used as shown in Fig. 1 and Table 1. In Fig. 1, the shear plane A includes the area A_1, A_2, A_3, A_4, A_5 and A_s. The friction plane Q includes Q_1, Q_2, and Q_3. In Fig. 2, geometrical wear of the cutting tool on the tool face is shown from the top view so as to define the type of wear on the tool edge: viz. a curve of radius R_3, a straight line and a curve of radii R_2, R_1 (R_1=R_2). The measurable values (i.e. h_1, h_2, h_3, h_4, l_1, l_2, l_3, l_4, and l_5) can be obtained by amplifying the profile projector screen by drawing the circumference of the tool edge before the cut, and again drawing the change after wear has occurred and can be obtained by the following equations:

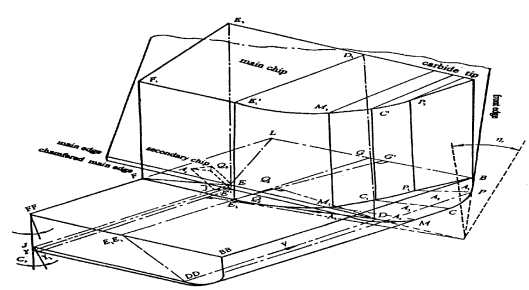

Fig. 1 Model of the chamfered main cutting Edge nose radius worn tool, $f > R$, $(R \neq 0)$

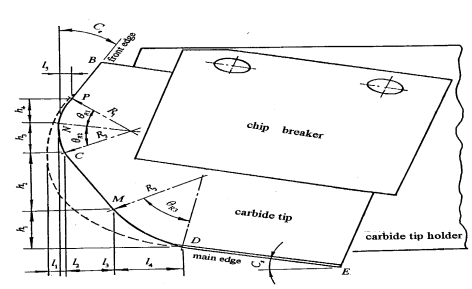

Fig. 2 Specifications of nose radius worn tool

$$A = A_1 + A_2 + A_3 + A_4 + A_5 + A_s \quad (1), \qquad Q = Q_1 + Q_2 + Q_3 \quad (2)$$

Table 1 Tool geometries specifications

Side cutting dge angle	tool no	Rake angle: α_{S1}, α_{S2}	Nose radius worn tools (R)
C_S=20 °	1	10 ° , -10 °	0.1, 0.3, 0.5, 1.0
C_S=20 °	2	20 ° , -20 °	0.1, 0.3, 0.5, 1.0
C_S=20 °	3	30 ° , -30 °	0.1, 0.3, 0.5, 1.0
C_S=30 °	4	10 ° , -10 °	0.1, 0.3, 0.5, 1.0
C_S=30 °	5	20 ° , -20 °	0.1, 0.3, 0.5, 1.0
C_S=30 °	6	30 ° , -30 °	0.1, 0.3, 0.5, 1.0
C_S=40 °	7	10 ° , -10 °	0.1, 0.3, 0.5, 1.0
C_S=40 °	8	20 ° , -20 °	0.1, 0.3, 0.5, 1.0
C_S=40 °	9	30 ° , -30 °	0.1, 0.3, 0.5, 1.0
tips			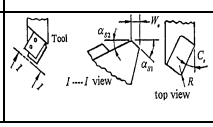

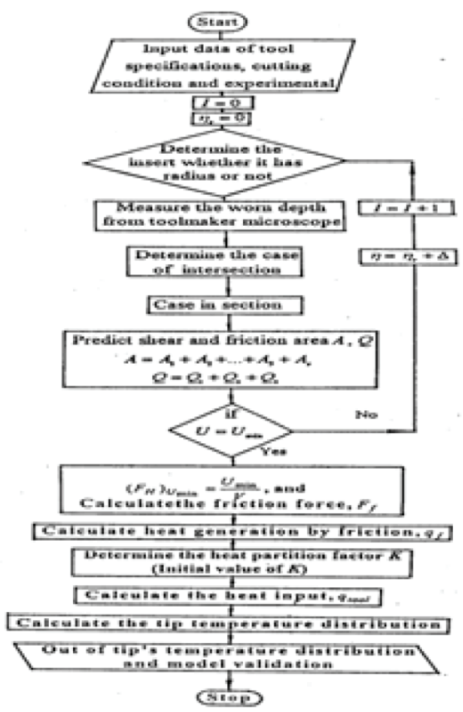

Fig. 3 Flow chart of heat calculate

2.1 Cutting Forces Calculation

Transformation equations used to obtain the normal (N_s) and shear forces (F_s) along the fiber direction in terms of the principal (F_c) and thrust components (F_t) are shown in Eqs. (4) and (5)

$$N_S = F_c \sin\theta + F_t \cos\theta \qquad (3)$$

$$F_c = t_0 A_0 \frac{\cos(\beta - r)}{\sin\theta\cos(\theta + \beta - r)} \qquad (4)$$

$$F_t = \tau_0 A_0 \frac{\cos(\beta - r)}{\sin\theta\cos(\theta + \beta - r)} \qquad (5)$$

$$\tau_s = \tau_{composite} = \tau_{fiber} V_f \qquad (6),$$

$$f_t = \tau_s t_1 \sin\beta / \cos(\phi + \beta - \alpha)\sin\phi \qquad (7)$$

Where the area of unreformed chip is A_0, β is the mean friction angle, r is the rake angle. By knowing the shear area A_0 of the unreformed chip, the shear strength τ_0 was calculated [3]. The shear energy per unit time (U_s) and the friction energy per unit time (U_f) were proposed as:

$$U_s = F_s V_s = \tau_s A V \cos\alpha_e / \cos(\phi_e - \alpha_e), \qquad (8)$$

$$F_S = F_c \cos\theta + F_t \sin\theta; \; V_s = V\cos\alpha_e / \cos(\phi_e - \alpha_e) \qquad (9)$$

$$U_f = F_t V_c = f_t \int_0^{B_1} d_b V_c = \tau_s \sin\beta V \cos\alpha_e Q$$
$$/[\cos(\phi_e + \beta - \alpha_e)\cos(\phi_e - \alpha_e)], \qquad (10)$$

$$U = U_s + U_f = V(F_H)_{U_{\min}} \qquad (11)$$

$$F_H = (F_H)_{U_{\min}} = U_{\min}/V = \{\tau_s \cos\alpha_e A / \cos(\phi_e - \alpha_e) +$$
$$\tau_s \sin\beta \cos\alpha_e Q / \cos(\phi_e + \beta - \alpha_e)\cos(\phi_e - \alpha_e)]\} \qquad (12)$$

$$F_t = \tau_s \sin\beta \cos\alpha_e Q / \cos(\phi_e + \beta - \alpha_e)\sin\phi_e \qquad (13)$$

$$\sigma_y = HB/\pi \quad (14); \qquad \tau_y = \sigma_y / 2 \qquad (15)$$

$$F_{HH} = (F_H)_M = (F_H)_{U_{\min}} \qquad (16)$$

$$F_{VV} = (F_V)_M \cos C_s - (F_T)_M \sin C_s \qquad (17)$$

$$F_{TT} = (F_T)_M \cos C_s + (F_V)_M \sin C_s \qquad (18)$$

2.2 Solid Modeling of Carbide Tip

To develop a 3D FEM model for thermal analysis, the tip cross-section profile perpendicular to the cutting edge was measured using a microscope, Solid Works™, was used to generate the tip body by sweeping the PCMO along the main cutting edge, as shown in Fig. 2.

2.3 Finite Element Model

The Abaqus™ is used in this study. The finite element mesh of the carbide tip is shown in Fig. 2, which was modeled by 58,000 four-node hexahedral elements. As shown in the top view of Fig. 4, 8*6 nodes are located on the projected contact length between the tool and the workpiece, 3 * 6 nodes are

located on the chamfered width of the main cutting edge, and 1*6 nodes are placed on flank wear.

2.4 Modified Carbide Tip Temperature Model

Magnitude of the tip's load is shown in the following Eqs. (19) and (20)

$K = U_f / A'$ (19), $A' = L_p(d + W_e + V_b)$ (20)

Where the area of friction force action is A', U_f is the friction energy, L_f is the contact length between the cutting edge and the workpiece, L_P is the projected contact length between the tool and the workpiece, as referred to in Fig. 5

$$\rho c \frac{\partial T}{\partial t} = k\frac{\partial^2 T}{\partial x^2} + k\frac{\partial^2 T}{\partial y^2} + k\frac{\partial^2 T}{\partial z^2} \quad (21)$$

$q_{tool} = Kq_f$ Li and Shih [4] (22)

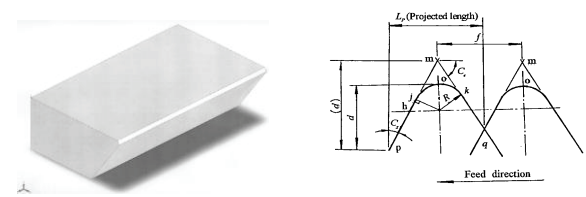

Fig. 4 Solid modelof tool (a)

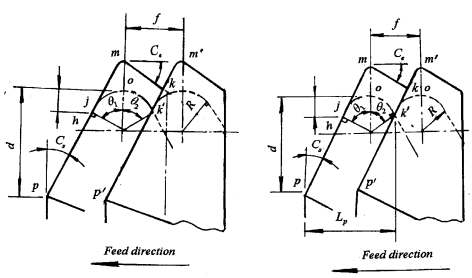

(b)

Fig. 5 Calculation the contact length (a) L_f , (b) L_p

where ρ is the density, c is the thermal conductivity, and k is the heat capacity. Assuming K is the heat partition factor to determine the ratio of heat transferred to the tool, the heat generation rate q_{tool} on each cutting edge is:

2.5 Inverse Heat Transfer Solution and Validation

The flowchart for inverse heat transfer solution of K was obtained by the Abaqus™ software and is summarized in Fig. 3. The Abaqus™ solver was used. By assuming a value for K, the spatial and temporal temperature distribution of the tip can be found. Finite element modeled temperature at specific infrared locations, as shown in Fig. 6(b) on the tip face. The estimated temperature at the same infrared location and time, $T_j^{ti}\big|_{\exp}$ determines the value of the objective function.

$$Obj(k) = \sum_{i=1}^{ni}\sum_{j=1}^{nj}(T_j^{ti}\big|_{\exp} - T_j^{ti}\big|_{est})^2 \text{ [4]} \quad (23)$$

3 EXPERIMENTAL PROCEDURES

Experimental set up is shown in Fig 6. Table 2 shows some of the physical and mechanical properties of GFRP [5]. The cutting tools used in the experiments are Sandvik H1P (*K type*) [6]. Tool composition: *WC 85.5%, TiC 7.5%, Ta (Nb)C 1% and Co 6 %*, HV =1740, density=10.3 g/cm^3 , thermal conductivity=23 $W/m-^oK$ and heat capacity= 200 $(J/Kg-^oK)$. The tool geometries showed in Table 1.

Fig. 6 Experimental set-up

4 RESULTS AND DISCUSSION

4.1 The Cutting Forces

Chang demonstrated in turning of GFRP with chamfered main cutting edge nose radius tools, the resultant cutting force, *Fr*, is about 15% less than that for unchamfered main cutting edge tools [7].

4.2 Temperature of Surface of Tip

Based on Li and Albert [4], according to Eqs. (20) to (21), the flowchart for inverse heat transfer solution of K is described in Fig. 3. After finding the value of K , the finite element model can be applied to calculate temperature at tips, the results are shown in Fig. 7.

5 CONCLUSIONS

The test investigated the cutting forces and cutting temperature during the turning of GFRP. Chamfered main cutting edge nose radius worn tools with C_S equals to 20˚, $\alpha_{S1}(\alpha_{S2}) = -10^{\circ}(10^{\circ})$ and nose radius R=0.3 mm, produce the lower cutting forces and lower cutting temperature. The FEM and Inverse heat transfer solution in tool temperature in CFRP turning is obtained and compared with experimental measurements. The good agreement demonstrates the accuracy of proposed model.

REFERENCES

[1] M. M. Schwartz, Composite materials handbook, second edition, McGraw-Hill, Inc., 1992, pp. 1.15-2.57

[2] S. B. Singamneni, A mixed solution for three-dimensional temperature distribution in turning inserts using finite and boundary element techniques, J. of Materials Processing Technology, 166 (2005) 98-106.

[3] M. E. Merchant, Basic mechanics of the metal cutting process, J. of Applied Mechanics, Trans. ASME, vol. 66(1944) 28-40.

[4] Rui Li and Albert J. Shih, Inverse heat transfer solution in tool temperature titanium drilling, mechanical engineering, University of Michigan Ann Arbor, 2005

[5] Liu C.C.,FRP and GTI composites, Golden Talent Industries Co. Ltd., Hsin-Chu, Taiwan, R.O.C., 2002, *J. of Mechanics (*SCI*)*, vol. 24, No. 4, pp. 241-252, 2008.

[6] K. J. A. Brookes, World Directory and Handbook of Hard metals, 5th edition, published by International carbide data hand book, United Kingdom, 1992, D172-175.

[7] C. S. Chang, "Turning of glass fiber reinforced plastics materials with chamfered main cutting carbide tools", J. of Materials Processing Technology, vol. 180, pp. 117-129, 2006.

Table 2 Properties of the work materials GFRP [5]

nominal form	density *gm/cm*^{3}	thermal conductivity *kCal/hr ℃*	fiber contain	coefficient of thermal expansion (10^{-6}/℃)	thermo-setting resins	hardness (Shore, *Hs*)	tensile strength (*kg/mm*^{2})	compare-ssive strength (*kg/mm*^{2})	Modulus tensile (*kg/mm*^{2})	shear strength (*kg/mm*^{2})
roving continuous strand	*1.8~2.1*	*0,21~0.28*	*75%*	*2~9*	*vinyl-ester*	*55~60*	*45~65*	*45~60*	*2000~4000*	*20*

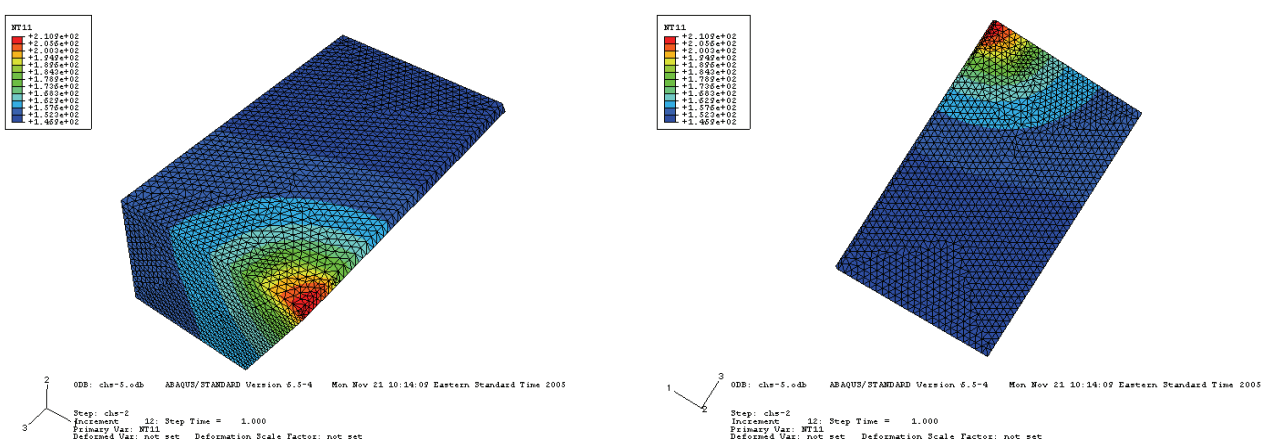

(a) (b)

Fig. 7 Temperature distribution with chamfered cutting edge inserts (a) heat flux (b) near the tool nose at C_S = 20˚, $\alpha_{S1}(\alpha_{S2}) = -10^{\circ}(10^{\circ})$, d=2.5mm, f=0.33mm/rev, and V=120 m/min (GFRP)